Review Article

Quantitative imaging methods in osteoporosis

Ling Oei[1,2], Fjorda Koromani[1,2], Fernando Rivadeneira[1,2], M. Carola Zillikens[1], Edwin H. G. Oei[3]

[1]Department of Internal Medicine, [2]Department of Radiology & Nuclear Medicine, [3]Department of Radiology & Nuclear Medicine, Erasmus MC, University Medical Center, Rotterdam, The Netherlands

Correspondence to: Edwin H. G. Oei, MD, PhD. Department of Radiology & Nuclear Medicine, Erasmus MC, University Medical Center, 's-Gravendijkwal 230, 3015 CE Rotterdam, The Netherlands. Email: e.oei@erasmusmc.nl.

Abstract: Osteoporosis is characterized by a decreased bone mass and quality resulting in an increased fracture risk. Quantitative imaging methods are critical in the diagnosis and follow-up of treatment effects in osteoporosis. Prior radiographic vertebral fractures and bone mineral density (BMD) as a quantitative parameter derived from dual-energy X-ray absorptiometry (DXA) are among the strongest known predictors of future osteoporotic fractures. Therefore, current clinical decision making relies heavily on accurate assessment of these imaging features. Further, novel quantitative techniques are being developed to appraise additional characteristics of osteoporosis including three-dimensional bone architecture with quantitative computed tomography (QCT). Dedicated high-resolution (HR) CT equipment is available to enhance image quality. At the other end of the spectrum, by utilizing post-processing techniques such as the trabecular bone score (TBS) information on three-dimensional architecture can be derived from DXA images. Further developments in magnetic resonance imaging (MRI) seem promising to not only capture bone micro-architecture but also characterize processes at the molecular level. This review provides an overview of various quantitative imaging techniques based on different radiological modalities utilized in clinical osteoporosis care and research.

Keywords: Quantitative imaging; osteoporosis; radiography; dual-energy X-ray absorptiometry (DXA); computed tomography (CT); magnetic resonance imaging (MRI); positron emission tomography (PET)

Submitted Nov 26, 2016. Accepted for publication Dec 14, 2016.
doi: 10.21037/qims.2016.12.13
View this article at: http://dx.doi.org/10.21037/qims.2016.12.13

Introduction

Osteoporosis is characterized by a decreased bone mass and quality resulting in an increased fracture risk. Quantitative imaging methods are of utmost importance in the diagnosis and follow-up of treatment effects in osteoporosis. The World Health Organization's (WHO) fracture risk assessment tool (FRAX®) is one of the well-established clinical risk score estimators enabling physicians to calculate the future risk of osteoporotic fractures in patients (1). Prior fracture (2-4) and bone mineral density (BMD) as quantitative parameters (5) are particularly strong predictors of future osteoporotic fractures. Therefore, when this information is available, these data can be entered into FRAX® along with epidemiological and clinical parameters to guide individualized therapeutic decision-making for patients. A high predicted risk justifies preventative treatment with anti-osteoporotic drugs. Although algorithms such as FRAX® represent major advances in clinical practice, clinicians should be aware that these calculations do not accommodate all known risk factors and there are more fracture determinants remaining to be discovered (6-8). Although FRAX® and the Garvan Fracture Risk Calculator provide estimates of which patients will sustain a fracture, these algorithms still underestimate observed fracture risk in at least half of patients (9). Also, there may be value in examining longitudinal follow-up assessments within a cohort over time, which is more feasible with objective quantitative measures. Ideally, we would like to expand our current

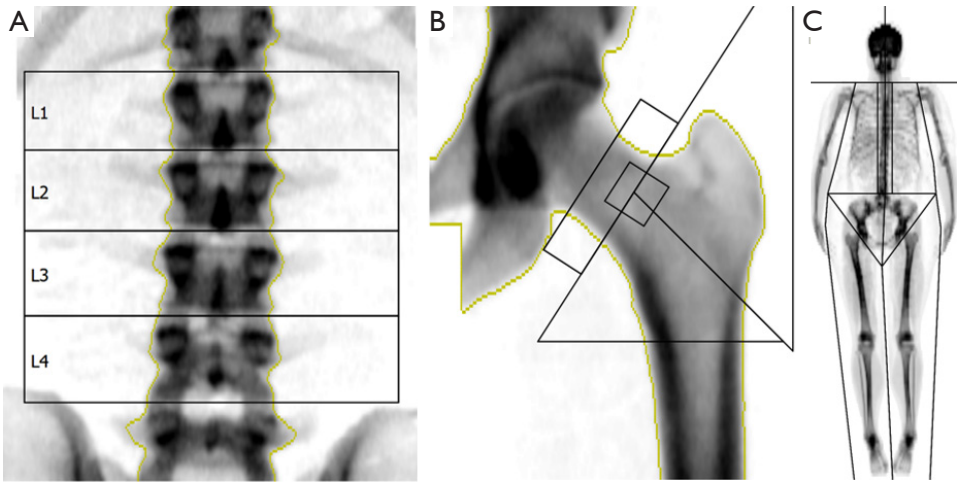

Figure 1 Example DXA images of the lumbar spine (A), femoral neck (B) and total body (C) with corresponding regions of interest in which BMD is measured. DXA, dual-energy X-ray absorptiometry; BMD, bone mineral density.

diagnostic panels by more advanced imaging to facilitate precision medicine and, subsequently, further improve the customization of healthcare tailored to the individual patient. Experimental assessments for osteoporosis are being developed in the research setting by either post-processing of radiographic or DXA data or involving more advanced imaging modalities such as computed tomography (CT) and magnetic resonance imaging (MRI) to appraise bone microarchitecture or bone geometry (i.e., biomechanical characteristics of a bone's size and shape) (10-16). This review discusses quantitative imaging methods for osteoporosis as applied in clinical care and scientific research.

Radiography

Unlike qualitative assessments of radiographs mostly applied for the diagnosis and follow-up of fractures, the application of quantitative radiographic methods in osteoporosis is declining, because these techniques have largely been replaced by DXA, as will be discussed below. Nevertheless, this paragraph will provide a brief summary of several techniques available. It is well-known that osteoporosis in appendicular long bones such as the proximal femur can be evident by cortical thinning and alterations of the trabecular pattern, which can be classified semi-quantitatively using for example the Singh index (17). Early X-ray based techniques for quantification of bone loss include radiogrammetry and radiographic absorptiometry. Radiogrammetry is a measurement of the cortical thickness of long bones, which has been used particularly in peripheral sites such as in the metacarpals (18). In radiographic absorptiometry, an aluminium phantom is placed next to the region of interest during X-ray acquisition. Subsequently, BMD is calibrated relative to the density of the phantom (19). Pulkkinen *et al.* extracted several geometrical and trabecular parameters from plain pelvic radiographs and related these to hip fracture risk (20). It has also been shown that bone density- and structure-related parameters can be calculated from radiographs of the proximal tibia in cadavers (21) and in subjects with osteoarthritis (22).

BMD by dual-energy X-ray absorptiometry (DXA)

Clinical measurement of BMD by DXA is currently the most widespread method to diagnose osteoporosis and evaluate the risk of fracture. DXA at the lumbar spine and femoral neck (*Figure 1A*,*B*) to measure BMD is nowadays a routine investigation in osteoporosis. DXA-measured BMD accounts for 60–70% of the variation in bone strength (23) and each standard deviation (SD) decrease of BMD is associated with a two-fold increase in fracture risk (1,24). Other skeletal sites or modes of measurement which are used more frequently in research settings are for example: total body (*Figure 1C*), (distal) radius, and skull. The BMD measured is measured in g/cm^2 but most commonly is expressed as the T-score, the number of SDs above or below the mean for a healthy 30-year-old adult of the same sex and ethnicity as the patient. Subsequently, osteoporosis is defined as a T-score ≤–2.5

and osteopenia as a T-score ≤–1.0 at any skeletal site. No upper reference value has been proposed, as the adverse health effects of having an increased BMD have been poorly studied. Intriguingly, the far majority of fractures occur in individuals without an abnormal clinically assessed BMD (24). Sensitivity and specificity for incident osteoporotic fractures are limited with an area under the ROC curve of 0.63 (25,26), as most fractures in the population distribution occur in mildly to moderately decreased BMD, i.e., osteopenia, or even at normal BMD values (24).

Moreover, several diseases are paradoxically known to be associated with a higher fracture risk despite a higher BMD, such as diabetes-related bone disease and degenerative disease (27,28). Theoretically, an individual with 5% higher femoral neck BMD would have a 10% decrease in fracture risk. Nonetheless, it has been shown that individuals with type 2 diabetes have 69% higher fracture risk than those without diabetes despite having higher BMD at the femoral neck and lumbar spine. Schwartz and colleagues established that the World Health Organization's fracture risk assessment tool (FRAX®) underestimates osteoporotic fracture risk in individuals with diabetes (29); this is why diabetes as a risk factor should be considered for inclusion in future iterations of FRAX® (30). Intriguingly, subjects with lumbar disc degeneration (LDD) have systematically higher BMD at the lumbar spine, femoral neck, skull, and consequently, at the total body measurement. In spite of this systematically higher BMD, persons with LDD are at higher risk of osteoporotic fractures, particularly males in whom LDD seems more severe (31). These observations suggest that more parameters are needed to define osteoporosis and obtain a better fracture risk assessment.

DXA—additional parameters

In recent years, several additional quantitative parameters have been described that can be extracted from existing DXA imaging data. For example, hip structural analysis can be performed on DXA images (32-34). Parameters that can be derived include cross-sectional area (CSA), cross-sectional moment of inertia (CSMI), and the section modulus, and using appropriate assumptions, one can estimate endocortical width and the cortical thickness (35). CSMI, as an estimation of the resistance of bone to bending, is calculated according to the formula: ([periosteal diameter/2]^4 – [medullary diameter/2]^4) × π/4 (36). Section modulus is calculated as CSMI divided by the greater of the measured distances from the center of mass to the medial or lateral surface, and is a measure of bending and torsional strength (35).

The trabecular bone score (TBS) seems a promising quantitative imaging parameter in osteoporosis, to some extent independent of DXA-BMD (37). Whereas DXA-BMD is a measure of bone quantity, TBS provides information on the biomechanics and microarchitecture which reflects trabecular structure (*Figure 2*). It is a grey-level texture measurement that utilizes an experimental variogram of two-dimensional (2D) projection images by measuring the rate of local variation in grey levels within 2D projection images to approximate three-dimensional (3D) bone microarchitecture (38). TBS is less expensive and more easily accessible than CT or MRI for wide-spread clinical implementation or as an outcome in large research studies. The very first TBS reports showed applications for the prediction of fracture risk in osteoporosis (39-41), have added value in those individuals with bone density outside of the osteoporosis range (42) and monitoring of treatment effects (43,44), and similarly, TBS may find an application in other conditions such as primary hyperparathyroidism (45), hypercortisolism (46), rheumatoid arthritis (47), and diabetes-related bone disease (48). A major advantage is that it can be derived from DXA scans using dedicated post-processing software. A recent meta-analysis demonstrated that the hazard ratio per 1 SD decrease in TBS increases by 1.44 for major osteoporotic fractures and seems of additional predictive value independent of the current FRAX model (49). TBS may be recognized as an independent endophenotype of osteoporosis and may have potential to guide clinical decision making similar to DXA-BMD in the future, which again would justify investigations into the determinants of TBS.

Quantitative ultrasound (QUS)

Over the past 30 years, ultrasonographic analysis, termed QUS, has been developed as a method of determining material properties of a variety of structures including the *in vivo* assessment of bone structure and fragility (50). In general, low-frequency ultrasonic velocity measurements are applied to the calcaneus without the use of ionizing radiation. Alternative peripheral sites to which QUS has been applied are the radius, tibiae and phalanges (51). Depending on the site of measurement, either of the two types of QUS is applied, i.e., horizontal transmission on the cortical layer of the bone, or longitudinal transmission

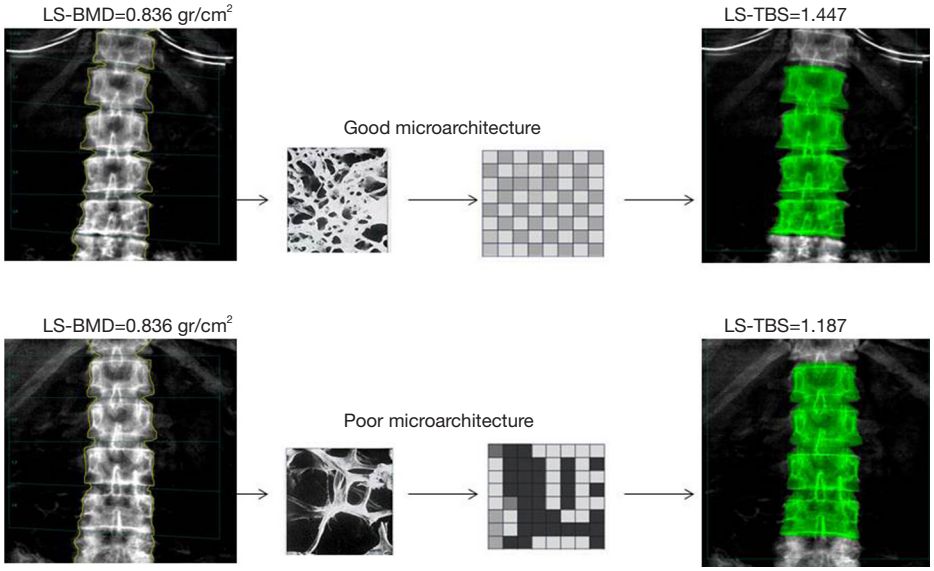

Figure 2 iDXA images of the spine, L1–L4 level of two individuals (top and bottom row); while LS-BMD values are the same for both, LS-TBS in the second subject is clearly lower compared to the first subject, corresponding to deteriorated microarchitecture of the vertebral body. LS-TBS value is derived by an algorithm that analyzes the spatial organization of pixel intensity, which in turn corresponds to the differences in the X-ray absorption power of an osteoporotic bone versus a normal trabecular pattern. (*Images partly adapted from* http://www.medimapsgroup.com/product/technology/).

measuring the speed of sound (52). The two main parameters are velocity of sound (VOS) and broadband ultrasound attenuation (BUA), and additional parameters obtained are stiffness index (SI), quantitative ultrasound index (QUI), amplitude-dependent speed of sound (AD-SOS), and estimated BMD (eBMD) (18,52). The speed of sound refers to the division of transmission time of the sound waves by the length of the body part studied in meter per second (m/s) (52). Broadband attenuation of sound refers to the energy which is absorbed by the tissues through which the sound waves are transmitted relative to the signal's frequency expressed in dB/MHz (52).

A meta-analysis by Moayyeri *et al*. showed that QUS parameters of the heel are associated with risk of hip fracture with relative risks per 1 SD decrease of 1.69 (95% CI: 1.43–2.00) for BUA, 1.96 (95% CI: 1.64–2.34) for SOS, 2.26 (95% CI: 1.71–2.99) for SI and 1.99 (95% CI: 1.49–2.67) for QUI (53). Analyses in the Canadian Multicentre Osteoporosis Study have been described for three alternative skeletal sites (distal radius, tibia, and phalanx) with a follow-up duration of 5 years (54).

Computed tomography (CT)

There is still a need for additional and more refined radiological imaging investigations for osteoporosis such as assessments based on CT. CT is more costly and requires more ionizing radiation than DXA and conventional radiography, but has numerous advantages as reviewed below. It is believed that there are skeletal-site specific effects for fracture risk including different roles for cortical versus trabecular bone, justifying efforts to separately analyze these entities (55). Quantitative computed tomography (QCT) yields volumetric 3D measurements by utilizing low dose scan protocols on a standard CT scanner or by performing high resolution-peripheral quantitative computed tomography (HR-)pQCT with the use of a dedicated extremity scanner (56). This allows more sophisticated analysis of cortical and trabecular bone, the imaging of trabecular structure and the application of finite element analysis (FEA) to model bone strength biomechanically (57-59). pQCT is also used in exploratory analyses for muscle, measuring for instance muscle CSA, muscle density, and intramuscular adipose tissue, which may be related to sarcopenia (60). In addition to the disadvantage of ionizing radiation, the analysis of CT imaging data can be complex and requires specialized software.

QCT is most commonly applied to the spine, and typically lumbar vertebral elements are evaluated (*Figure 3A,B*); Other skeletal sites include the hip (*Figure 3C,D,E*)

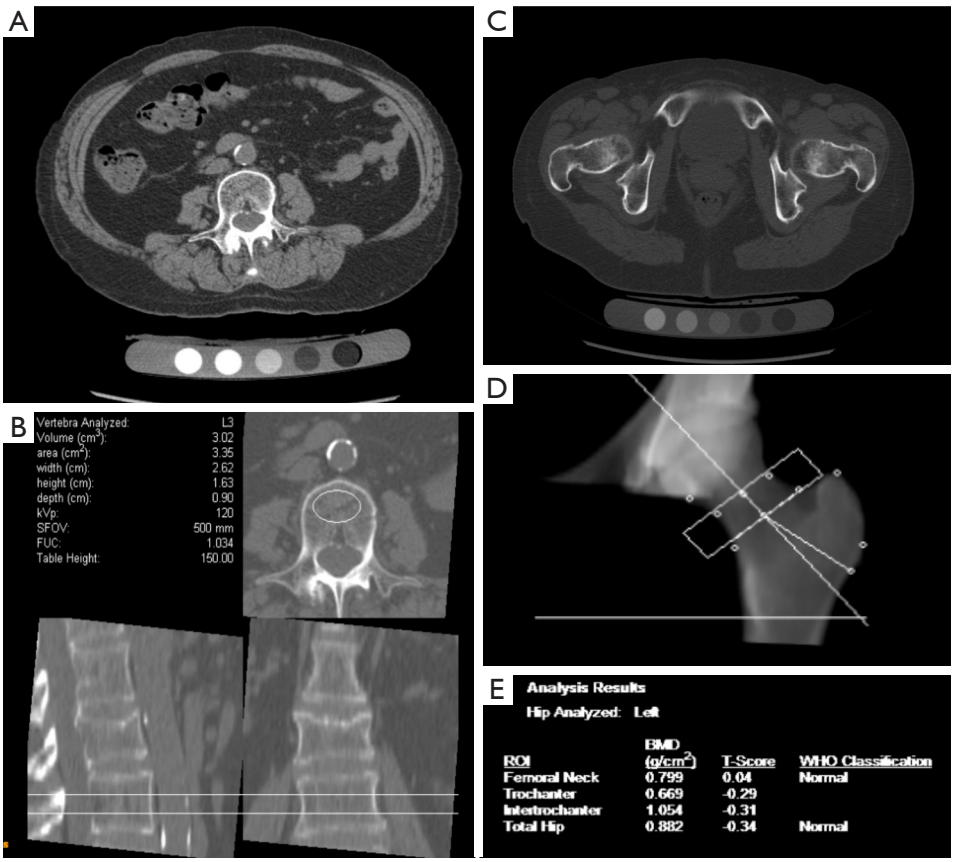

Figure 3 Quantitative computed tomography (QCT) of the lumbar spine and the hip. Source image obtained in the lumbar spine of a 65-year-old female (A), with definition of region of interest in vertebra L3 yielding a BMD (68.4 mg/cc) in the osteoporotic range according to the guidelines of the American Board of radiologists (B). Source image obtained in the hip of a 76-year-old female (C), with definition of regions of interest in the left femoral neck (D) and subsequent bone mineral density (BMD) analysis showing normal bone densities (E). (*Images courtesy of Thomas Link, MD PhD, University of California at San Francisco, Dept. of Radiology and Biomedical imaging*).

and the forearm (61). Simply measuring X-ray attenuation expressed as Hounsfield units (HU) to derive BMD has been evaluated (62,63), but ideally the tissue density of the analyzed volume is calibrated to units of equivalent concentration of a hydroxyapatite phantom in g/cm^3 yielding the BMD values (64). Volumes of interest are defined and a distinction is made between cortical, trabecular and integral volumes (65). QCT-based vertebral bone measurements are associated with vertebral fractures (66,67), and may outperform DXA-based measurements (68). Several studies have been performed in the proximal femur showing a difference of FEA parameters between hip fracture and vertebral fracture cases versus controls (69-71).

HR-pQCT is applied to the tibia or (distal) radius with simultaneous scanning of a hydroxyapatite calibration phantom, obtaining measurements within trabecular and cortical compartments (12). In cortical bone, standard analysis comprises cortical thickness (Ct.Th) in mm, cortical porosity (Ct.Po) as a percentage relative to the cortical pore volume (Ct.Po.V), and cortical bone volume (Ct.BV) in mm^3 (72,73). It has been shown that with increasing age most bone loss is cortical due to predominantly intracortical remodelling (74). This results in increased spatial distribution, number and size of pores (75). In trabecular bone, standard analysis includes quantifying structural properties of trabecular bone, such as bone volume fraction (BV/TV), which is derived from trabecular BMD (Tb.BMD), average number of trabeculae (Tb.N), average trabecular thickness (Tb.Th), and average trabecular separation (Tb.Sp) (76). Associations have been demonstrated for different HR-pQCT measurements at the tibia and radius for vertebral and any-type of fractures (77-81).

Volumetric assessments with HR-pQCT also have added value in complex phenotypes such as diabetic bone disease. DXA-based studies showed that type 2 diabetes patients with worse glycemic control have paradoxically higher BMD and thicker femoral cortices in narrower bones in spite of a higher fracture risk (82). A study using HR-pQCT reported that the cortical porosity in type 2 diabetic patients was up to twice that of controls at the radius (73). This supports the hypothesis that an inefficient redistribution of bone mass, accumulation of microcracks and cortical porosity reflecting impaired bone repair give rise to fragility in apparently "strong" bones on 2D assessments in inadequately controlled diabetes. Subsequently, Patsch *et al*. showed in a four-group comparison of type 2 diabetes patients with and without fragility fractures to controls with and without fractures that cortical porosity is specific to those type 2 diabetes patients that fracture (83). Moreover, an innovative investigation utilizing *in vivo* microindentation testing of the tibia showed that patients with type 2 diabetes have reduced serum markers of bone turnover and lower bone material strength than controls (84). In this same study the average glycemic level over the previous ten years was negatively correlated with bone material strength (84). It would be desirable to investigate these phenomena with (pQ)CT on a larger population scale. Medical evidence is still too limited to warrant large-scale implementation of CT in clinical practice at this point (85,86). In the future, diagnostics and therapeutics may separately target cortical versus trabecular bone compartments.

MRI

High-resolution (HR) MRI may help in directly or indirectly assessing the structure of bone (87). MRI is relatively more costly and time-consuming, and produces a lower spatial resolution than CT. However, a major advantage is that it does not require ionizing radiation. Furthermore, MRI has great potential for detailed characterization of bone at the micro-architectural and molecular level, as reviewed below.

Histomorphometry is the gold standard for assessing bone, because it is the only method for the direct analysis of bone cells and their activities (88). Yet, even in the clinical setting bone biopsies are rarely used to diagnose and manage patients with osteoporosis, because of their invasiveness (89). Molecular imaging, the *in vivo* characterization and measurement of biological processes at the cellular and molecular level, is being hailed as the next great advance for imaging (90). Technical improvements in MRI are necessary for human application, particularly with regard to maximizing signal-to-noise ratio and spatial resolution within clinically acceptable scan times. This is a prerequisite for the introduction into large-scale population imaging studies and clinical practice in the future to aid the analysis of a large variety of musculoskeletal disorders including osteoporosis.

Inferences can be made about trabecular bone structure from HR MRI. Osteoporosis patients with and without fractures compared to individuals without osteoporosis have been evaluated for different MRI-derived texture parameters of bone, and differences between these groups were demonstrated at the distal radius and calcaneus (91-93).

One of the few MRI-based studies in diabetic bone disease reported greater trabecular heterogeneity in subjects with type 2 diabetes mellitus than in healthy controls (94). More MRI studies in diabetic bone disease are necessary given the recent insights regarding the impact of diabetes on bone quality.

Indirect MRI methods used for evaluation of the bone structure include MRI spectroscopy aiming to visualize the osseous structure or the changes in the structure at a molecular level without the need of contrast agents. Proton-magnetic resonance spectroscopy (^{1}H-MRS) is considered the MRI gold standard for bone marrow fat quantification, and point-resolved spectroscopy (PRESS) and stimulated echo acquisition mode (STEAM) single-voxel ^{1}H-MRS pulse sequences have been commonly used for the characterization of the fat spectrum in the bone marrow at the pelvis, spine, and hip (95). Images are acquired using dedicated coils to detect and quantify frequency signals of water, lipids, and other metabolites, expressed as universal ppm (parts per million) units with evaluation of areas under the peaks. In addition to qualitative interpretation, (semi-)quantitative analysis is in use such as scaling of ratios to unsuppressed water or to noise (96,97). Increased emphasis on quantitative assessment instead of qualitative dichotomization of metabolite content by MRS has been advocated (98). Measurement quality and awareness of possible artifacts are important in MRS (99), and adequate distinction of the molecular peaks and regions of interest can be technically challenging (95); corrections can be applied to minimize confounding effects (100).

Direct methods include chemical shift imaging, diffusion-weighted imaging, and perfusion MRI. Chemical shift imaging aims to separately detect protons that process with similar yet slightly different frequencies, namely, those of

water and fat (101). A study evaluating the reproducibility of signal intensity index (SII) measurements in healthy volunteers with MRI systems from different vendors and with different field strengths found intra- and inter-observer correlation coefficients ranging from 0.82 to 0.98 (102). In osteoporosis, the few studies performed until now have primarily assessed the bone marrow (103-105). Diffusion-weighted imaging measures the Brownian motion of water at a microscopic level and provides information on cellularity and cellular integrity expressed in the apparent diffusion coefficient (ADC) (101). A review article discussing diffusion-weighted imaging in musculoskeletal radiology has been published in this journal before (106). Also for diffusion-weighted imaging, most studies in osteoporosis have focused on the bone marrow (107-109). A few studies reported diffusion-weighted MR imaging parameters to be associated with BMD (110,111). One study has examined ADC values before and after vertebroplasty and found that high preoperative ADC was predictive of the occurrence of new compression fractures (112); replication studies are necessary. Different methods are used for perfusion imaging, of which the dynamic contrast-enhanced MRI (DCE-MRI) technique is the most commonly implemented (101). Possible analytical approaches to DCE-MRI data include time-intensity curves, enhancement patterns over time and pharmacokinetic modeling approaches to quantify blood flow. Quantitative outcomes of diffusion-weighted imaging and dynamic contrast-enhanced MRI have been reported to be different between acute osteoporotic vertebral fractures from normal appearing vertebrae (113). Furthermore, maximum enhancement [E(max)] and enhancement slope [E(slope)] are significantly decreased in osteoporosis in at least the femurs and vertebrae (114-118). Quantitative parameters of blood flow were studied with DCE-MRI in osteoporotic patients with acute vertebral fracture compared to a control group (119). Plasma flow (mL/100 mL/min) quantifies the volume of plasma flowing through the region of interest per unit time; plasma volume (mL/100 mL) corresponds to the volume of the plasma per tissue volume in the region of interest and extraction flow (mL/100 mL/min) characterizes the net flow between the plasma and the interstitial space (extracellular and extravascular space). These perfusion parameters were decreased in normal-appearing vertebral bone marrow of osteoporosis patients compared to controls, but they were found to increase in acute vertebral fractures.

A shortcoming of MRI is that, due to its short T2 relaxation time, no signal from cortical bone is acquired with conventional MRI pulse sequences (120). Hence, sequences with ultrashort echo time are needed to capture signals of those tissues which exhibit short T2 (e.g., cortical bones, tendons, ligaments, menisci and myelin) (121). This may be overcome with novel ultrashort or zero time to echo (UTE/ZTE) MRI techniques (*Figure 4*). ^{1}H, being the most abundant isotope of hydrogen, is present in bone water and these signals can be acquired by aforementioned techniques. The ^{1}H signal arises from different pools, distinguishable by their relaxation times. Relatively free water within large pores has the longest T2 relaxation times; water in small pores has greater surface to volume ratios, experiences greater surface relaxation and thus has a shorter T2 relaxation time (122). Protons bound to bone matrix are more tightly restricted in movement and have shorter T2 relaxation times. A variety of UTE pulse sequences have been developed capable of depicting signal from different water pools in bone (*Figure 5*) and quantitating the amount of water by means of T2* relaxometry. The field is making steps in translating experience from animal and cadaveric experiments to *in vivo* human studies (123-126). As bone water is present mainly in the pore system of bone, this parameter provides a surrogate measure for porosity, and it has been demonstrated that cortical bone water concentration is greater in postmenopausal women than in premenopausal women (127).

Bone marrow fat imaging

Bone marrow fat may be affected by diseases such as osteoporosis and diabetic bone disease (128). The bone marrow fat volume can be measured (129). Further, bone marrow fat composition can be examined, regarding presence and types of hydrogen bonds, where unsaturated fats contain at least one double bond and saturated fats have the maximum number of hydrogens bonded to carbons. This can be evaluated with MRS, dual energy QCT (130,131), T1-weighted and occasionally T2-weighted MRI (132). The average coefficient of variation for vertebral bone marrow fat fraction on spectroscopy has been reported at 1.7% (97). The correlation between the marrow fat fraction obtained with MRS and that obtained with dual-energy CT has been reported as high as r=0.91 (133). Vertebral marrow fat content is significantly increased in osteoporosis compared to osteopenia or normal bone density as evaluated by higher fat fractions on MRS and lower ADC by diffusion weighted MR (134). An ancillary study in the population-based Age Gene/Environment Susceptibility (AGES) cohort found that higher marrow fat

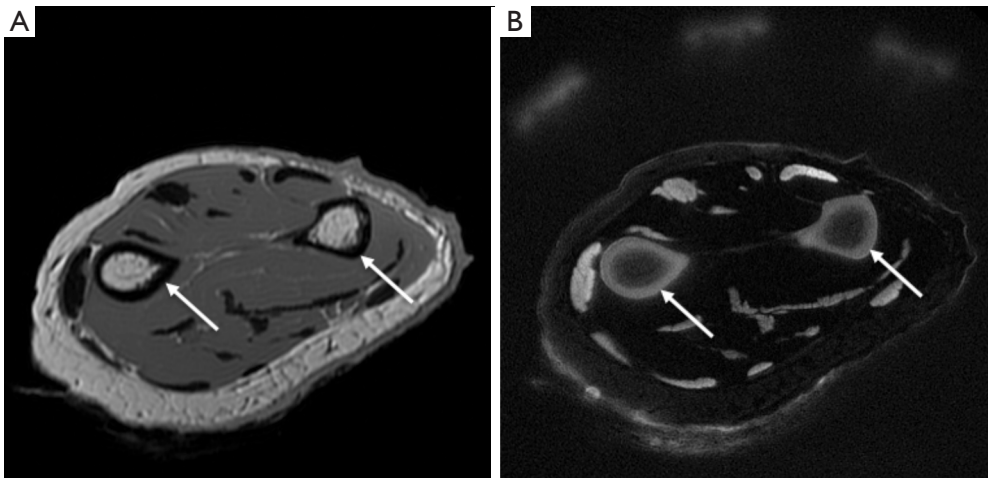

Figure 4 MRI of a cadaveric forearm. Cortical bone produces a signal void on a conventional fast-spin echo (FSE) sequence (A), while signal is detected from cortical bone with the use of an inversion recovery ultrashort echo time (IR UTE, TR/TI 300/120 ms) pulse sequence. MRI, magnetic resonance imaging. (*Images courtesy of Jiang Du, PhD, University of California at San Diego, Dept. of Radiology*).

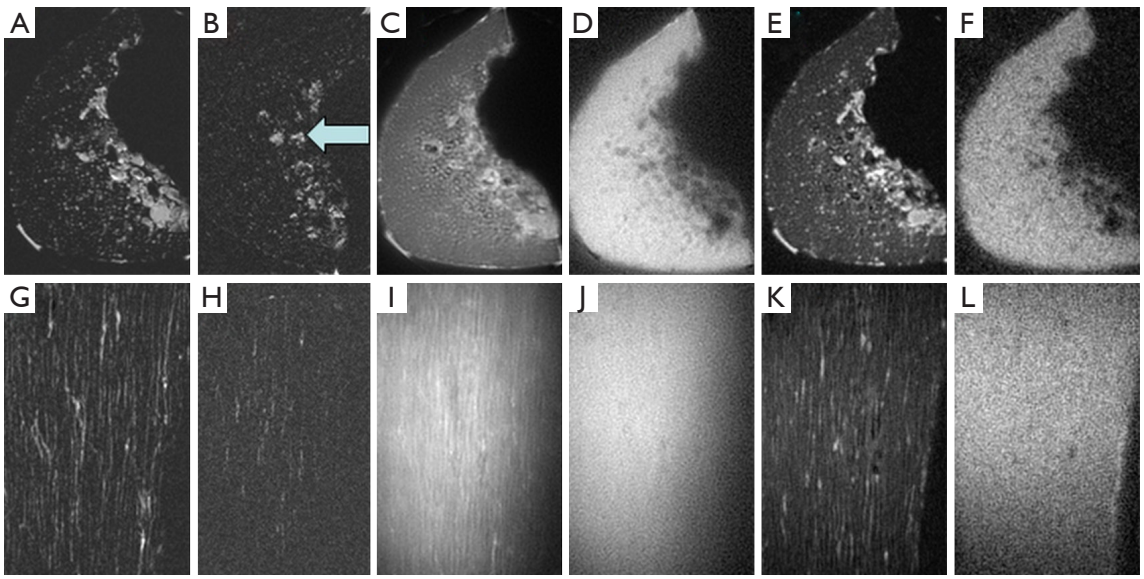

Figure 5 Axial (1st row) and sagittal (2nd row) imaging of a cortical bone sample with 2D FSE (A,G), 2D GRE (B,H), 2D UTE (C,I), 2D IR-UTE (D,J), 3D UTE (E,K) and 3D IR-UTE (F,L) sequences. Free water in the Haversian canals is detected by both FSE, 2D and 3D UTE sequences. Both 2D and 3D IR-UTE show a relatively uniform bright signal, consistent with only bound water being detected. GRE shows little signal for both bound and free water in cortical bone. The bright signal in (B) corresponds to marrow fat (arrow). (*Images courtesy of Jiang Du, PhD, University of California at San Diego, Dept. of Radiology*).

assessed by MRS correlated with lower trabecular BMD in women and higher marrow fat was associated with prevalent vertebral fracture in men (135). Validation of these results should be pursued.

Dixon quantitative chemical shift MRI (QCSI) relies on phase shifts created by fat-water resonance frequency differences to separate water from fat (136). Studies have reported good reproducibility for Dixon QCSI for measuring the bone marrow fat fraction in the L1–L4 vertebral bodies and this measurement seems independent

of DXA-BMD (137).

A small study in subjects with disuse osteoporosis has demonstrated morphological changes in the bone marrow at the lower limb such as reinforcement of trabecular lines, subchondral fat content, signal intensity and vasculature (138). Further quantitative texture analysis on this subject in larger samples may be worthwhile.

Combined QCT and MRS studies have demonstrated that the prevalence of fragility fractures is associated with lower unsaturation levels and higher saturation levels of bone marrow fat, in which the participants with diabetes with fractures have the lowest marrow unsaturation and highest saturation (139). In contrast to controls without diabetes, higher mean vertebral bone marrow fat content is significantly correlated with visceral adipose tissue and HbA1C in persons with type 2 diabetes, representing worse metabolic profiles (140). The concept of high-saturated fat-associated adipose inflammation and insulin resistance has been proposed; however, underlying molecular mechanisms remain to be elucidated.

Positron emission tomography (PET)

Application of PET/CT in the field of osteoporosis is still limited. In certain clinical fracture cases where CT and MRI images are inconclusive in differentiating benign from malignant etiologies, PET/CT can be acquired, which can also discover additional skeletal or extra-skeletal metastases (141). The standardized uptake value (SUV), a dimensionless parameter, is commonly used as a relative measure of FDG tissue uptake with correction for the amount of injected FDG and the patient size (142). Further, bone fracture healing can be visualized by PET/CT, but this has predominantly been studied in animal models (143-146). Zooming in further, in ^{18}F-Fluoride PET scanning it is believed that PET intensity reflects the activities of osteoblasts and osteoclasts, and at least in animal experiments, microdamage can be detected (147). Regional bone perfusion and turnover studies with bone turnover markers as a reference have been performed comparing different skeletal sites in treatment-naïve and patients with osteoporosis on treatment with various anti-osteoporotic agents (148-154). The long term precision reflected by the coefficients of variation (12.2–26.6%) and intraclass correlation (0.44–0.85) for ^{18}F-Fluoride PET parameters has been reported to be equivalent to that observed for biochemical bone turnover markers (155). It has been hypothesized that PET/CT may be useful in atypical femoral fracture patients, but supportive research data is needed (156).

No reports on the utilization of PET/MRI in osteoporosis have been published to date. Neither has diabetic bone disease been studied with PET/MRI in humans; a small study comparing diabetic and healthy pigs found a significant inverse correlation between vertebral bone marrow glucose uptake and fat content (157). Nonetheless, the first PET/MRI studies to detect and characterize osseous metabolic abnormalities in osteoarthritis are being done where PET/MRI may detect metabolic abnormalities in subchondral bone, which appear normal on MRI (158). Development of MRI quantitative imaging techniques is an exciting area of research deserving further explorations.

Vertebral fractures

The occurrence of fracture is without doubt the most important clinical outcome in osteoporosis. Vertebral fractures may go misdiagnosed as the clinical presentation can be aspecific. Moreover, as two thirds of vertebral fractures do not give clinical symptoms, these may be only detected on radiological imaging (159). Nevertheless, vertebral fractures increase the risk of new vertebral fracture up to five-fold and the risk of other fragility fractures two- to four-fold (160). Drugs available for the treatment of osteoporosis are highly effective, with the most potent bisphosphonate zoledronic acid reducing the risk of vertebral fractures by 76% and of non-vertebral fractures by 24% (161). Therefore, another valuable evaluation in osteoporosis is vertebral fracture assessment (VFA) on mostly lateral DXA or radiography (*Figure 6*). Vertebral fractures can be detected on other modalities such as CT or MRI as well. The differentiation between vertebral fractures of benign and malignant etiologies has been reviewed elsewhere (162).

Fractures can be classified according to skeletal site and shape, and quantified according to the amount of height loss and the number of fractures. However, there is currently no gold standard for osteoporotic vertebral fracture diagnosis (163). Several radiological scoring methods exist, each using different criteria for diagnosing and grading fractures. These assessment methods for osteoporotic vertebral fractures including quantitative morphometry (QM) analyses have been reviewed extensively elsewhere (164,165). Frequently used are methods based on (semi) QM evaluating vertebral

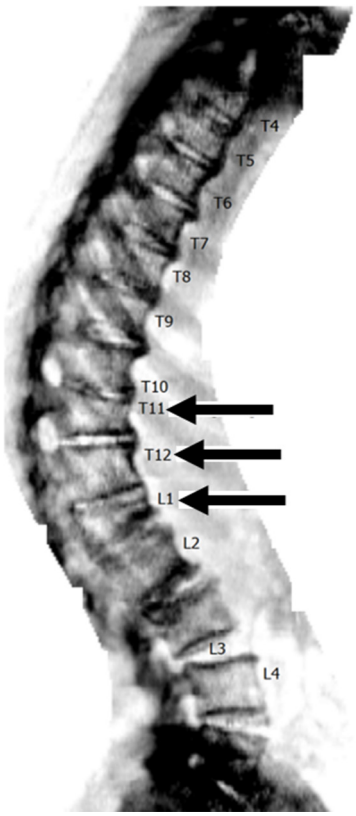

Figure 6 Vertebral fracture assessment (VFA) on lateral DXA demonstrates multiple wedge-shaped vertebral fractures in a patient with osteoporosis. DXA, dual-energy X-ray absorptiometry.

height (166) or the algorithm-based qualitative (ABQ) method (167) mainly judging endplate integrity regardless of vertebral height reduction. Further work is needed to reveal which of the discordant cases are actually clinically relevant; evaluating the predictive ability of the different definitions with different relevant outcomes like future non-vertebral and vertebral fractures, and mortality are desirable. All vertebral fractures are deformities, but not all vertebral deformities are fractures. There are a number of differential diagnoses that have to be considered in individuals with vertebral deformities (168), such as Scheuermann's disease and degenerative changes (167). Scheuermann's disease is a form of osteochondrosis of the spine of unknown etiology characterized by increased posterior rounding of the thoracic spine in association with structural deformity of the vertebral elements (169,170).

Phenotype definition is a cornerstone of epidemiological research into vertebral fracture risk to prevent bias hampering discoveries (171-173). Moreover, merely measuring vertebral heights in clinical practice frequently leads to misdiagnosis of fracture in non-osteoporotic conditions including Scheuermann's disease (174-176). Simultaneous assessment of vertebral heights together with endplate integrity may correctly differentiate these cases. One of the major advantages of software-assisted QM is the level of detail of the data recording (165). If more evidence supporting the ABQ method will be put forward, it will be worthwhile to explore if endplate integrity can be captured in software-assisted assessments based on computer-based morphometric recognition. In addition to improvement of the radiological vertebral fracture definition by itself, clearer criteria for non-fracture deformities differential diagnosis are necessary. A clear and correct fracture definition is crucial, because vertebral fractures form an integral part of clinical decision making to initiate anti-osteoporotic drugs or to switch to more potent and expensive agents in case of fractures under current therapy.

Conclusions

This review has summarized quantitative imaging methods in osteoporosis, where current clinical practice most frequently utilizes assessments from DXA and conventional radiography. Correct interpretation is crucial as treatment decisions are taken based on these outcomes. Further technical developments are ongoing to expand the richness of data obtained from these modalities. Finally, potentially novel application of quantitative parameters from ultrasound, CT, MRI and PET are underway in clinical and research settings.

Acknowledgements

None.

Footnote

Conflicts of Interest: The authors have no conflicts of interest to declare.

References

1. Dawson-Hughes B, Tosteson AN, Melton LJ 3rd, Baim S, Favus MJ, Khosla S, Lindsay RL; National Osteoporosis Foundation Guide Committee. Implications of absolute fracture risk assessment for osteoporosis practice guidelines in the USA. Osteoporos Int 2008;19:449-58.

2. van der Klift M, de Laet CE, McCloskey EV, Johnell O, Kanis JA, Hofman A, Pols HA. Risk factors for incident vertebral fractures in men and women: the Rotterdam Study. J Bone Miner Res 2004;19:1172-80.
3. Kanis JA, Johnell O, De Laet C, Johansson H, Oden A, Delmas P, Eisman J, Fujiwara S, Garnero P, Kroger H, McCloskey EV, Mellstrom D, Melton LJ, Pols H, Reeve J, Silman A, Tenenhouse A. A meta-analysis of previous fracture and subsequent fracture risk. Bone 2004;35:375-82.
4. Black DM, Arden NK, Palermo L, Pearson J, Cummings SR. Prevalent vertebral deformities predict hip fractures and new vertebral deformities but not wrist fractures. Study of Osteoporotic Fractures Research Group. J Bone Miner Res 1999;14:821-8.
5. Johnell O, Kanis JA, Oden A, Johansson H, De Laet C, Delmas P, Eisman JA, Fujiwara S, Kroger H, Mellstrom D, Meunier PJ, Melton LJ 3rd, O'Neill T, Pols H, Reeve J, Silman A, Tenenhouse A. Predictive value of BMD for hip and other fractures. J Bone Miner Res 2005;20:1185-94.
6. Silverman SL, Calderon AD. The utility and limitations of FRAX: A US perspective. Curr Osteoporos Rep 2010;8:192-7.
7. Estrada K, Styrkarsdottir U, Evangelou E, et al. Genome-wide meta-analysis identifies 56 bone mineral density loci and reveals 14 loci associated with risk of fracture. Nat Genet 2012;44:491-501.
8. Oei L, Hsu YH, Styrkarsdottir U, et al. A genome-wide copy number association study of osteoporotic fractures points to the 6p25.1 locus. J Med Genet 2014;51:122-31.
9. van Geel TA, Eisman JA, Geusens PP, van den Bergh JP, Center JR, Dinant GJ. The utility of absolute risk prediction using FRAX® and Garvan Fracture Risk Calculator in daily practice. Maturitas 2014;77:174-9.
10. Burghardt AJ, Link TM, Majumdar S. High-resolution computed tomography for clinical imaging of bone microarchitecture. Clin Orthop 2011;469:2179-93.
11. Krug R, Burghardt AJ, Majumdar S, Link TM. High-resolution imaging techniques for the assessment of osteoporosis. Radiol Clin North Am 2010;48:601-21.
12. Link TM. Osteoporosis imaging: state of the art and advanced imaging. Radiology 2012;263:3-17.
13. Van Goethem JW, Maes M, Ozsarlak O, van den Hauwe L, Parizel PM. Imaging in spinal trauma. Eur Radiol 2005;15:582-90.
14. Wilmink JT. MR imaging of the spine: trauma and degenerative disease. Eur Radiol 1999;9:1259-66.
15. Bouxsein ML, Karasik D. Bone geometry and skeletal fragility. Curr Osteoporos Rep 2006;4:49-56.
16. Beck TJ, Ruff CB, Warden KE, Scott WW Jr, Rao GU. Predicting femoral neck strength from bone mineral data. A structural approach. Invest Radiol 1990;25:6-18.
17. Singh M, Nagrath AR, Maini PS. Changes in trabecular pattern of the upper end of the femur as an index of osteoporosis. J Bone Joint Surg Am 1970;52:457-67.
18. Pocock NA. Quantitative diagnostic methods in osteoporosis: a review. Australas Radiol 1998;42:327-34.
19. Genant HK, Engelke K, Fuerst T, Glüer CC, Grampp S, Harris ST, Jergas M, Lang T, Lu Y, Majumdar S, Mathur A, Takada M. Noninvasive assessment of bone mineral and structure: state of the art. J Bone Miner Res 1996;11:707-30.
20. Pulkkinen P, Partanen J, Jalovaara P, Nieminen MT, Jämsä T. Combination of radiograph-based trabecular and geometrical parameters can discriminate cervical hip fractures from controls in individuals with BMD in non-osteoporotic range. Bone 2011;49:290-4.
21. Hirvasniemi J, Thevenot J, Kokkonen HT, Finnilä MA, Venäläinen MS, Jämsä T, Korhonen RK, Töyräs J, Saarakkala S. Correlation of Subchondral Bone Density and Structure from Plain Radiographs with Micro Computed Tomography Ex Vivo. Ann Biomed Eng 2016;44:1698-709.
22. Hirvasniemi J, Thevenot J, Immonen V, Liikavainio T, Pulkkinen P, Jämsä T, Arokoski J, Saarakkala S. Quantification of differences in bone texture from plain radiographs in knees with and without osteoarthritis. Osteoarthritis Cartilage 2014;22:1724-31.
23. Ammann P, Rizzoli R. Bone strength and its determinants. Osteoporos Int 2003;14 Suppl 3:S13-8.
24. Schuit SC, van der Klift M, Weel AE, de Laet CE, Burger H, Seeman E, Hofman A, Uitterlinden AG, van Leeuwen JP, Pols HA. Fracture incidence and association with bone mineral density in elderly men and women: the Rotterdam Study. Bone 2004;34:195-202.
25. Kanis JA, Oden A, Johnell O, Johansson H, De Laet C, Brown J, Burckhardt P, Cooper C, Christiansen C, Cummings S, Eisman JA, Fujiwara S, Glüer C, Goltzman D, Hans D, Krieg MA, La Croix A, McCloskey E, Mellstrom D, Melton LJ 3rd, Pols H, Reeve J, Sanders K, Schott AM, Silman A, Torgerson D, van Staa T, Watts NB, Yoshimura N. The use of clinical risk factors enhances the performance of BMD in the prediction of hip and osteoporotic fractures in men and women. Osteoporos Int 2007;18:1033-46.
26. Leslie WD, Lix LM, Johansson H, Oden A, McCloskey E,

Kanis JA; Manitoba Bone Density Program. Independent clinical validation of a Canadian FRAX tool: fracture prediction and model calibration. J Bone Miner Res 2010;25:2350-8.
27. Ma L, Oei L, Jiang L, Estrada K, Chen H, Wang Z, Yu Q, Zillikens MC, Gao X, Rivadeneira F. Association between bone mineral density and type 2 diabetes mellitus: a meta-analysis of observational studies. Eur J Epidemiol 2012;27:319-32.
28. Oei L, Rivadeneira F, Zillikens MC, Oei EH. Diabetes, diabetic complications, and fracture risk. Curr Osteoporos Rep 2015;13:106-15.
29. Schwartz AV, Vittinghoff E, Bauer DC, Hillier TA, Strotmeyer ES, Ensrud KE, Donaldson MG, Cauley JA, Harris TB, Koster A, Womack CR, Palermo L, Black DM; Study of Osteoporotic Fractures (SOF) Research Group.; Osteoporotic Fractures in Men (MrOS) Research Group.; Health, Aging, and Body Composition (Health ABC) Research Group. Association of BMD and FRAX score with risk of fracture in older adults with type 2 diabetes. JAMA 2011;305:2184-92.
30. Giangregorio LM, Leslie WD, Lix LM, Johansson H, Oden A, McCloskey E, Kanis JA. FRAX underestimates fracture risk in patients with diabetes. J Bone Miner Res 2012;27:301-8.
31. Castaño-Betancourt MC, Oei L, Rivadeneira F, de Schepper EI, Hofman A, Bierma-Zeinstra S, Pols HA, Uitterlinden AG, Van Meurs JB. Association of lumbar disc degeneration with osteoporotic fractures; the Rotterdam study and meta-analysis from systematic review. Bone 2013;57:284-9.
32. Oei L, Campos-Obando N, Dehghan A, Oei EH, Stolk L, van Meurs JB, Hofman A, Uitterlinden AG, Franco OH, Zillikens MC, Rivadeneira F. Dissecting the relationship between high-sensitivity serum C-reactive protein and increased fracture risk: the Rotterdam Study. Osteoporos Int 2014;25:1247-54.
33. Muka T, Trajanoska K, Kiefte-de Jong JC, Oei L, Uitterlinden AG, Hofman A, Dehghan A, Zillikens MC, Franco OH, Rivadeneira F. The Association between Metabolic Syndrome, Bone Mineral Density, Hip Bone Geometry and Fracture Risk: The Rotterdam Study. PloS One 2015;10:e0129116.
34. van der Eerden BC, Oei L, Roschger P, Fratzl-Zelman N, Hoenderop JG, van Schoor NM, Pettersson-Kymmer U, Schreuders-Koedam M, Uitterlinden AG, Hofman A, Suzuki M, Klaushofer K, Ohlsson C, Lips PJ, Rivadeneira F, Bindels RJ, van Leeuwen JP. TRPV4 deficiency causes sexual dimorphism in bone metabolism and osteoporotic fracture risk. Bone 2013;57:443-54.
35. Structural trends in the aging femoral neck and proximal shaft: analysis of the Third National Health and Nutrition Examination Survey dual-energy X-ray absorptiometry data. J Bone Miner Res 2000;15:2297-304.
36. Ahlborg HG, Johnell O, Turner CH, Rannevik G, Karlsson MK. Bone loss and bone size after menopause. N Engl J Med 2003;349:327-34.
37. Silva BC, Leslie WD, Resch H, Lamy O, Lesnyak O, Binkley N, McCloskey EV, Kanis JA, Bilezikian JP. Trabecular bone score: a noninvasive analytical method based upon the DXA image. J Bone Miner Res 2014;29:518-30.
38. Pothuaud L, Carceller P, Hans D. Correlations between grey-level variations in 2D projection images (TBS) and 3D microarchitecture: applications in the study of human trabecular bone microarchitecture. Bone 2008;42:775-87.
39. Briot K, Paternotte S, Kolta S, Eastell R, Reid DM, Felsenberg D, Glüer CC, Roux C. Added value of trabecular bone score to bone mineral density for prediction of osteoporotic fractures in postmenopausal women: the OPUS study. Bone 2013;57:232-6.
40. Hans D, Goertzen AL, Krieg MA, Leslie WD. Bone microarchitecture assessed by TBS predicts osteoporotic fractures independent of bone density: the Manitoba study. J Bone Miner Res 2011;26:2762-9.
41. Iki M, Tamaki J, Kadowaki E, Sato Y, Dongmei N, Winzenrieth R, Kagamimori S, Kagawa Y, Yoneshima H. Trabecular bone score (TBS) predicts vertebral fractures in Japanese women over 10 years independently of bone density and prevalent vertebral deformity: the Japanese Population-Based Osteoporosis (JPOS) cohort study. J Bone Miner Res 2014;29:399-407.
42. Boutroy S, Hans D, Sornay-Rendu E, Vilayphiou N, Winzenrieth R, Chapurlat R. Trabecular bone score improves fracture risk prediction in non-osteoporotic women: the OFELY study. Osteoporos Int 2013;24:77-85.
43. Krieg MA, Aubry-Rozier B, Hans D, Leslie WD; Manitoba Bone Density Program. Effects of anti-resorptive agents on trabecular bone score (TBS) in older women. Osteoporos Int 2013;24:1073-8.
44. Popp AW, Guler S, Lamy O, Senn C, Buffat H, Perrelet R, Hans D, Lippuner K. Effects of zoledronate versus placebo on spine bone mineral density and microarchitecture assessed by the trabecular bone score in postmenopausal women with osteoporosis: a three-year study. J Bone Miner Res 2013;28:449-54.

45. Eller-Vainicher C, Filopanti M, Palmieri S, Ulivieri FM, Morelli V, Zhukouskaya VV, Cairoli E, Pino R, Naccarato A, Verga U, Scillitani A, Beck-Peccoz P, Chiodini I. Bone quality, as measured by trabecular bone score, in patients with primary hyperparathyroidism. Eur J Endocrinol 2013;169:155-62.
46. Eller-Vainicher C, Morelli V, Ulivieri FM, Palmieri S, Zhukouskaya VV, Cairoli E, Pino R, Naccarato A, Scillitani A, Beck-Peccoz P, Chiodini I. Bone quality, as measured by trabecular bone score in patients with adrenal incidentalomas with and without subclinical hypercortisolism. J Bone Miner Res 2012;27:2223-30.
47. Bréban S, Briot K, Kolta S, Paternotte S, Ghazi M, Fechtenbaum J, Roux C. Identification of rheumatoid arthritis patients with vertebral fractures using bone mineral density and trabecular bone score. J Clin Densitom 2012;15:260-6.
48. Leslie WD, Aubry-Rozier B, Lamy O, Hans D; Manitoba Bone Density Program. TBS (trabecular bone score) and diabetes-related fracture risk. J Clin Endocrinol Metab 2013;98:602-9.
49. McCloskey EV, Odén A, Harvey NC, et al. A Meta-Analysis of Trabecular Bone Score in Fracture Risk Prediction and Its Relationship to FRAX. J Bone Miner Res 2016;31:940-8.
50. Moayyeri A, Hsu YH, Karasik D, Estrada K, Xiao SM, Nielson C, et al. Genetic determinants of heel bone properties: genome-wide association meta-analysis and replication in the GEFOS/GENOMOS consortium. Hum Mol Genet 2014;23:3054-68.
51. Adams JE. Advances in bone imaging for osteoporosis. Nat Rev Endocrinol 2013;9:28-42.
52. Chin KY, Ima-Nirwana S. Calcaneal quantitative ultrasound as a determinant of bone health status: what properties of bone does it reflect? Int J Med Sci 2013;10:1778-83.
53. Moayyeri A, Adams JE, Adler RA, Krieg MA, Hans D, Compston J, Lewiecki EM. Quantitative ultrasound of the heel and fracture risk assessment: an updated meta-analysis. Osteoporos Int 2012;23:143-53.
54. Olszynski WP, Brown JP, Adachi JD, Hanley DA, Ioannidis G, Davison KS; CaMos Research Group. Multisite quantitative ultrasound for the prediction of fractures over 5 years of follow-up: the Canadian Multicentre Osteoporosis Study. J Bone Miner Res 2013;28:2027-34.
55. Kemp JP, Medina-Gomez C, Estrada K, et al. Phenotypic dissection of bone mineral density reveals skeletal site specificity and facilitates the identification of novel loci in the genetic regulation of bone mass attainment. PLoS Genet 2014;10:e1004423.
56. Adams JE. Quantitative computed tomography. Eur J Radiol 2009;71:415-24.
57. Boutroy S, Van Rietbergen B, Sornay-Rendu E, Munoz F, Bouxsein ML, Delmas PD. Finite element analysis based on in vivo HR-pQCT images of the distal radius is associated with wrist fracture in postmenopausal women. J Bone Miner Res 2008;23:392-9.
58. Amin S, Kopperdhal DL, Melton LJ 3rd, Achenbach SJ, Therneau TM, Riggs BL, Keaveny TM, Khosla S. Association of hip strength estimates by finite-element analysis with fractures in women and men. J Bone Miner Res 2011;26:1593-600.
59. Chevalier Y, Quek E, Borah B, Gross G, Stewart J, Lang T, Zysset P. Biomechanical effects of teriparatide in women with osteoporosis treated previously with alendronate and risedronate: results from quantitative computed tomography-based finite element analysis of the vertebral body. Bone 2010;46:41-8.
60. Erlandson MC, Lorbergs AL, Mathur S, Cheung AM. Muscle analysis using pQCT, DXA and MRI. Eur J Radiol 2016;85:1505-11.
61. Engelke K, Libanati C, Fuerst T, Zysset P, Genant HK. Advanced CT based in vivo methods for the assessment of bone density, structure, and strength. Curr Osteoporos Rep 2013;11:246-55.
62. Pompe E, de Jong PA, de Jong WU, Takx RA, Eikendal AL, Willemink MJ, Oudkerk M, Budde RP, Lammers JW, Mohamed Hoesein FA. Inter-observer and inter-examination variability of manual vertebral bone attenuation measurements on computed tomography. Eur Radiol 2016;26:3046-53.
63. Pickhardt PJ, Pooler BD, Lauder T, del Rio AM, Bruce RJ, Binkley N. Opportunistic screening for osteoporosis using abdominal computed tomography scans obtained for other indications. Ann Intern Med 2013;158:588-95.
64. Nielson CM, Liu CT, Smith AV, et al. Novel Genetic Variants Associated With Increased Vertebral Volumetric BMD, Reduced Vertebral Fracture Risk, and Increased Expression of SLC1A3 and EPHB2. J Bone Miner Res 2016;31:2085-97.
65. Engelke K, Mastmeyer A, Bousson V, Fuerst T, Laredo JD, Kalender WA. Reanalysis precision of 3D quantitative computed tomography (QCT) of the spine. Bone 2009;44:566-72.
66. Anderson DE, Demissie S, Allaire BT, Bruno AG, Kopperdahl DL, Keaveny TM, Kiel DP, Bouxsein ML.

The associations between QCT-based vertebral bone measurements and prevalent vertebral fractures depend on the spinal locations of both bone measurement and fracture. Osteoporos Int 2014;25:559-66.
67. Wang X, Sanyal A, Cawthon PM, Palermo L, Jekir M, Christensen J, Ensrud KE, Cummings SR, Orwoll E, Black DM; Osteoporotic Fractures in Men (MrOS) Research Group., Keaveny TM. Prediction of new clinical vertebral fractures in elderly men using finite element analysis of CT scans. J Bone Miner Res 2012;27:808-16.
68. Yu W, Glüer CC, Grampp S, Jergas M, Fuerst T, Wu CY, Lu Y, Fan B, Genant HK. Spinal bone mineral assessment in postmenopausal women: a comparison between dual X-ray absorptiometry and quantitative computed tomography. Osteoporos Int 1995;5:433-9.
69. Keyak JH, Sigurdsson S, Karlsdottir G, Oskarsdottir D, Sigmarsdottir A, Zhao S, Kornak J, Harris TB, Sigurdsson G, Jonsson BY, Siggeirsdottir K, Eiriksdottir G, Gudnason V, Lang TF. Male-female differences in the association between incident hip fracture and proximal femoral strength: a finite element analysis study. Bone 2011;48:1239-45.
70. Kopperdahl DL, Aspelund T, Hoffmann PF, Sigurdsson S, Siggeirsdottir K, Harris TB, Gudnason V, Keaveny TM. Assessment of incident spine and hip fractures in women and men using finite element analysis of CT scans. J Bone Miner Res 2014;29:570-80.
71. Orwoll ES, Marshall LM, Nielson CM, Cummings SR, Lapidus J, Cauley JA, Ensrud K, Lane N, Hoffmann PR, Kopperdahl DL, Keaveny TM; Osteoporotic Fractures in Men Study Group. Finite element analysis of the proximal femur and hip fracture risk in older men. J Bone Miner Res 2009;24:475-83.
72. Ostertag A, Peyrin F, Fernandez S, Laredo JD, de Vernejoul MC, Chappard C. Cortical measurements of the tibia from high resolution peripheral quantitative computed tomography images: a comparison with synchrotron radiation micro-computed tomography. Bone 2014;63:7-14.
73. Burghardt AJ, Issever AS, Schwartz AV, Davis KA, Masharani U, Majumdar S, Link TM. High-resolution peripheral quantitative computed tomographic imaging of cortical and trabecular bone microarchitecture in patients with type 2 diabetes mellitus. J Clin Endocrinol Metab 2010;95:5045-55.
74. Zebaze RM, Ghasem-Zadeh A, Bohte A, Iuliano-Burns S, Mirams M, Price RI, Mackie EJ, Seeman E. Intracortical remodelling and porosity in the distal radius and post-mortem femurs of women: a cross-sectional study. Lancet 2010;375:1729-36.
75. Nirody JA, Cheng KP, Parrish RM, Burghardt AJ, Majumdar S, Link TM, Kazakia GJ. Spatial distribution of intracortical porosity varies across age and sex. Bone 2015;75:88-95.
76. Manhard MK, Nyman JS, Does MD. Advances in imaging approaches to fracture risk evaluation. Transl Res 2016. [Epub ahead of print].
77. Stein EM, Liu XS, Nickolas TL, Cohen A, McMahon DJ, Zhou B, Zhang C, Kamanda-Kosseh M, Cosman F, Nieves J, Guo XE, Shane E. Microarchitectural abnormalities are more severe in postmenopausal women with vertebral compared to nonvertebral fractures. J Clin Endocrinol Metab 2012;97:E1918-1926.
78. Sundh D, Mellström D, Nilsson M, Karlsson M, Ohlsson C, Lorentzon M. Increased Cortical Porosity in Older Men With Fracture. J Bone Miner Res 2015;30:1692-700.
79. Bala Y, Zebaze R, Ghasem-Zadeh A, Atkinson EJ, Iuliano S, Peterson JM, Amin S, Bjørnerem Å, Melton LJ 3rd, Johansson H, Kanis JA, Khosla S, Seeman E. Cortical porosity identifies women with osteopenia at increased risk for forearm fractures. J Bone Miner Res 2014;29:1356-62.
80. Ohlsson C, Sundh D, Wallerek A, Nilsson M, Karlsson M, Johansson H, Mellström D, Lorentzon M. Cortical bone area predicts incident fractures independently of areal bone mineral density in older men. J Clin Endocrinol Metab 2016. [Epub ahead of print].
81. Szulc P, Boutroy S, Vilayphiou N, Chaitou A, Delmas PD, Chapurlat R. Cross-sectional analysis of the association between fragility fractures and bone microarchitecture in older men: the STRAMBO study. J Bone Miner Res 2011;26:1358-67.
82. Oei L, Zillikens MC, Dehghan A, Buitendijk GH, Castaño-Betancourt MC, Estrada K, Stolk L, Oei EH, van Meurs JB, Janssen JA, Hofman A, van Leeuwen JP, Witteman JC, Pols HA, Uitterlinden AG, Klaver CC, Franco OH, Rivadeneira F. High bone mineral density and fracture risk in type 2 diabetes as skeletal complications of inadequate glucose control: the Rotterdam Study. Diabetes Care 2013;36:1619-28.
83. Patsch JM, Burghardt AJ, Yap SP, Baum T, Schwartz AV, Joseph GB, Link TM. Increased cortical porosity in type 2 diabetic postmenopausal women with fragility fractures. J Bone Miner Res 2013;28:313-24.
84. Farr JN, Drake MT, Amin S, Melton LJ 3rd, McCready LK, Khosla S. In vivo assessment of bone quality in postmenopausal women with type 2 diabetes. J Bone

Miner Res 2014;29:787-95.
85. Engelke K, Adams JE, Armbrecht G, Augat P, Bogado CE, Bouxsein ML, Felsenberg D, Ito M, Prevrhal S, Hans DB, Lewiecki EM. Clinical use of quantitative computed tomography and peripheral quantitative computed tomography in the management of osteoporosis in adults: the 2007 ISCD Official Positions. J Clin Densitom 2008;11:123-62.
86. Zemel B, Bass S, Binkley T, Ducher G, Macdonald H, McKay H, Moyer-Mileur L, Shepherd J, Specker B, Ward K, Hans D. Peripheral quantitative computed tomography in children and adolescents: the 2007 ISCD Pediatric Official Positions. J Clin Densitom 2008;11:59-74.
87. Gokalp G, Mutlu FS, Yazici Z, Yildirim N. Evaluation of vertebral bone marrow fat content by chemical-shift MRI in osteoporosis. Skeletal Radiol 2011;40:577-85.
88. Iwaniec UT, Wronski TJ, Turner RT. Histological analysis of bone. Methods Mol Biol 2008;447:325-41.
89. Malluche HH, Mawad H, Monier-Faugere MC. Bone biopsy in patients with osteoporosis. Curr Osteoporos Rep 2007;5:146-52.
90. Hoffman JM, Gambhir SS. Molecular imaging: the vision and opportunity for radiology in the future. Radiology 2007;244:39-47.
91. Majumdar S, Genant HK, Grampp S, Newitt DC, Truong VH, Lin JC, Mathur A. Correlation of trabecular bone structure with age, bone mineral density, and osteoporotic status: in vivo studies in the distal radius using high resolution magnetic resonance imaging. J Bone Miner Res 1997;12:111-8.
92. Majumdar S, Link TM, Augat P, Lin JC, Newitt D, Lane NE, Genant HK. Trabecular bone architecture in the distal radius using magnetic resonance imaging in subjects with fractures of the proximal femur. Magnetic Resonance Science Center and Osteoporosis and Arthritis Research Group. Osteoporos Int 1999;10:231-9.
93. Link TM, Majumdar S, Augat P, Lin JC, Newitt D, Lu Y, Lane NE, Genant HK. In vivo high resolution MRI of the calcaneus: differences in trabecular structure in osteoporosis patients. J Bone Miner Res 1998;13:1175-82.
94. Pritchard JM, Giangregorio LM, Atkinson SA, Beattie KA, Inglis D, Ioannidis G, Punthakee Z, Adachi JD, Papaioannou A. Association of larger holes in the trabecular bone at the distal radius in postmenopausal women with type 2 diabetes mellitus compared to controls. Arthritis Care Res (Hoboken) 2012;64:83-91.
95. Cordes C, Baum T, Dieckmeyer M, Ruschke S, Diefenbach MN, Hauner H, Kirschke JS, Karampinos DC. MR-Based Assessment of Bone Marrow Fat in Osteoporosis, Diabetes, and Obesity. Front Endocrinol (Lausanne) 2016;7:74.
96. Bredella MA, Gill CM, Gerweck AV, Landa MG, Kumar V, Daley SM, Torriani M, Miller KK. Ectopic and serum lipid levels are positively associated with bone marrow fat in obesity. Radiology 2013;269:534-41.
97. Li X, Kuo D, Schafer AL, Porzig A, Link TM, Black D, Schwartz AV. Quantification of vertebral bone marrow fat content using 3 Tesla MR spectroscopy: reproducibility, vertebral variation, and applications in osteoporosis. J Magn Reson Imaging 2011;33:974-9.
98. Deshmukh S, Subhawong T, Carrino JA, Fayad L. Role of MR spectroscopy in musculoskeletal imaging. Indian J Radiol Imaging 2014;24:210-6.
99. Kreis R. Issues of spectral quality in clinical 1H-magnetic resonance spectroscopy and a gallery of artifacts. NMR Biomed 2004;17:361-81.
100. Dieckmeyer M, Ruschke S, Cordes C, Yap SP, Kooijman H, Hauner H, Rummeny EJ, Bauer JS, Baum T, Karampinos DC. The need for T_2 correction on MRS-based vertebral bone marrow fat quantification: implications for bone marrow fat fraction age dependence. NMR Biomed 2015;28:432-9.
101. Fayad LM, Jacobs MA, Wang X, Carrino JA, Bluemke DA. Musculoskeletal tumors: how to use anatomic, functional, and metabolic MR techniques. Radiology 2012;265:340-56.
102. Xiao Z, Li J, Li C, Zhang Y, She D, Cao D. Chemical shift MR imaging in the lumbar vertebra: the effect of field strength, scanner vendors and flip angles in repeatability of signal intensity index measurement. BMC Med Imaging 2016;16:64.
103. Régis-Arnaud A, Guiu B, Walker PM, Krausé D, Ricolfi F, Ben Salem D. Bone marrow fat quantification of osteoporotic vertebral compression fractures: comparison of multi-voxel proton MR spectroscopy and chemical-shift gradient-echo MR imaging. Acta Radiol 2011;52:1032-6.
104. Li G, Xu Z, Gu H, Li X, Yuan W, Chang S, Fan J, Calimente H, Hu J. Comparison of chemical shift-encoded water-fat MRI and MR spectroscopy in quantification of marrow fat in postmenopausal females. J Magn Reson Imaging 2017;45:66-73.
105. Ragab Y, Emad Y, Gheita T, Mansour M, Abou-Zeid A, Ferrari S, Rasker JJ. Differentiation of osteoporotic and neoplastic vertebral fractures by chemical shift {in-phase and out-of phase} MR imaging. Eur J Radiol 2009;72:125-33.

106. Bhojwani N, Szpakowski P, Partovi S, Maurer MH, Grosse U, von Tengg-Kobligk H, Zipp-Partovi L, Fergus N, Kosmas C, Nikolaou K, Robbin MR. Diffusion-weighted imaging in musculoskeletal radiology-clinical applications and future directions. Quant Imaging Med Surg 2015;5:740-53.
107. Sung JK, Jee WH, Jung JY, Choi M, Lee SY, Kim YH, Ha KY, Park CK. Differentiation of acute osteoporotic and malignant compression fractures of the spine: use of additive qualitative and quantitative axial diffusion-weighted MR imaging to conventional MR imaging at 3.0 T. Radiology 2014;271:488-98.
108. Liu Y, Tang GY, Tang RB, Peng YF, Li W. Assessment of bone marrow changes in postmenopausal women with varying bone densities: magnetic resonance spectroscopy and diffusion magnetic resonance imaging. Chin Med J (Engl) 2010;123:1524-7.
109. Biffar A, Baur-Melnyk A, Schmidt GP, Reiser MF, Dietrich O. Quantitative analysis of the diffusion-weighted steady-state free precession signal in vertebral bone marrow lesions. Invest Radiol 2011;46:601-9.
110. Koyama H, Yoshihara H, Kotera M, Tamura T, Sugimura K. The quantitative diagnostic capability of routine MR imaging and diffusion-weighted imaging in osteoporosis patients. Clin Imaging 2013;37:925-9.
111. Rebuzzi M, Vinicola V, Taggi F, Sabatini U, Wehrli FW, Capuani S. Potential diagnostic role of the MRI-derived internal magnetic field gradient in calcaneus cancellous bone for evaluating postmenopausal osteoporosis at 3T. Bone 2013;57:155-63.
112. Sugimoto T, Tanigawa N, Ikeda K, Ohmura N, Maehara M, Kariya S, Kojima H, Komemushi A, Ha-Kawa SK, Saito Y, Tajika A, Kinoshita T, Sawada S. Diffusion-weighted imaging for predicting new compression fractures following percutaneous vertebroplasty. Acta Radiol 2008;49:419-26.
113. Biffar A, Sourbron S, Dietrich O, Schmidt G, Ingrisch M, Reiser MF, Baur-Melnyk A. Combined diffusion-weighted and dynamic contrast-enhanced imaging of patients with acute osteoporotic vertebral fractures. Eur J Radiol 2010;76:298-303.
114. Wang YX, Griffith JF, Kwok AW, Leung JC, Yeung DK, Ahuja AT, Leung PC. Reduced bone perfusion in proximal femur of subjects with decreased bone mineral density preferentially affects the femoral neck. Bone 2009;45:711-5.
115. Griffith JF, Yeung DK, Tsang PH, Choi KC, Kwok TC, Ahuja AT, Leung KS, Leung PC. Compromised bone marrow perfusion in osteoporosis. J Bone Miner Res 2008;23:1068-75.
116. Tokuda O, Hayashi N, Taguchi K, Matsunaga N. Dynamic contrast-enhanced perfusion MR imaging of diseased vertebrae: analysis of three parameters and the distribution of the time-intensity curve patterns. Skeletal Radiol 2005;34:632-8.
117. Kanchiku T, Taguchi T, Toyoda K, Fujii K, Kawai S. Dynamic contrast-enhanced magnetic resonance imaging of osteoporotic vertebral fracture. Spine (Phila Pa 1976) 2003;28:2522-6; discussion 2.
118. Griffith JF, Yeung DK, Antonio GE, Lee FK, Hong AW, Wong SY, Lau EM, Leung PC. Vertebral bone mineral density, marrow perfusion, and fat content in healthy men and men with osteoporosis: dynamic contrast-enhanced MR imaging and MR spectroscopy. Radiology 2005;236:945-51.
119. Biffar A, Schmidt GP, Sourbron S, D'Anastasi M, Dietrich O, Notohamiprodjo M, Reiser MF, Baur-Melnyk A. Quantitative analysis of vertebral bone marrow perfusion using dynamic contrast-enhanced MRI: initial results in osteoporotic patients with acute vertebral fracture. J Magn Reson Imaging 2011;33:676-83.
120. Robson MD, Gatehouse PD, Bydder M, Bydder GM. Magnetic resonance: an introduction to ultrashort TE (UTE) imaging. J Comput Assist Tomogr 2003;27:825-46.
121. Latta P, Starčuk Z Jr, Gruwel ML, Weber MH, Tomanek B. K-space trajectory mapping and its application for ultrashort Echo time imaging. Magn Reson Imaging 2016;36:68-76.
122. Seifert AC, Wehrli FW. Solid-State Quantitative (1)H and (31)P MRI of Cortical Bone in Humans. Curr Osteoporos Rep 2016;14:77-86.
123. Chen J, Carl M, Ma Y, Shao H, Lu X, Chen B, Chang EY, Wu Z, Du J. Fast volumetric imaging of bound and pore water in cortical bone using three-dimensional ultrashort-TE (UTE) and inversion recovery UTE sequences. NMR Biomed 2016;29:1373-80.
124. Chen J, Chang EY, Carl M, Ma Y, Shao H, Chen B, Wu Z, Du J. Measurement of bound and pore water T1 relaxation times in cortical bone using three-dimensional ultrashort echo time cones sequences. Magn Reson Med 2016. [Epub ahead of print].
125. Manhard MK, Horch RA, Gochberg DF, Nyman JS, Does MD. In Vivo Quantitative MR Imaging of Bound and Pore Water in Cortical Bone. Radiology 2015;277:927.
126. Ma L, Meng Q, Chen Y, Zhang Z, Sun H, Deng D. Preliminary use of a double-echo pulse sequence with 3D

ultrashort echo time in the MRI of bones and joints. Exp Ther Med 2013;5:1471-5.
127. Techawiboonwong A, Song HK, Leonard MB, Wehrli FW. Cortical bone water: in vivo quantification with ultrashort echo-time MR imaging. Radiology 2008;248:824-33.
128. Rubin MR, Patsch JM. Assessment of bone turnover and bone quality in type 2 diabetic bone disease: current concepts and future directions. Bone Res 2016;4:16001.
129. Shen W, Scherzer R, Gantz M, Chen J, Punyanitya M, Lewis CE, Grunfeld C. Relationship between MRI-measured bone marrow adipose tissue and hip and spine bone mineral density in African-American and Caucasian participants: the CARDIA study. J Clin Endocrinol Metab 2012;97:1337-46.
130. Goodsitt MM, Johnson RH, Chesnut CH. A new set of calibration standards for estimating the fat and mineral content of vertebrae via dual energy QCT. Bone Miner 1991;13:217-33.
131. Goodsitt MM, Hoover P, Veldee MS, Hsueh SL. The composition of bone marrow for a dual-energy quantitative computed tomography technique. A cadaver and computer simulation study. Invest Radiol 1994;29:695-704.
132. Schwartz AV. Marrow fat and bone: review of clinical findings. Front Endocrinol (Lausanne) 2015;6:40.
133. Bredella MA, Daley SM, Kalra MK, Brown JK, Miller KK, Torriani M. Marrow Adipose Tissue Quantification of the Lumbar Spine by Using Dual-Energy CT and Single-Voxel (1)H MR Spectroscopy: A Feasibility Study. Radiology 2015;277:230-5.
134. Agrawal K, Agarwal Y, Chopra RK, Batra A, Chandra R, Thukral BB. Evaluation of MR Spectroscopy and Diffusion-Weighted MRI in Postmenopausal Bone Strength. Cureus 2015;7:e327.
135. Schwartz AV, Sigurdsson S, Hue TF, Lang TF, Harris TB, Rosen CJ, Vittinghoff E, Siggeirsdottir K, Sigurdsson G, Oskarsdottir D, Shet K, Palermo L, Gudnason V, Li X. Vertebral bone marrow fat associated with lower trabecular BMD and prevalent vertebral fracture in older adults. J Clin Endocrinol Metab 2013;98:2294-300.
136. Bley TA, Wieben O, François CJ, Brittain JH, Reeder SB. Fat and water magnetic resonance imaging. J Magn Reson Imaging 2010;31:4-18.
137. Maas M, Akkerman EM, Venema HW, Stoker J, Den Heeten GJ. Dixon quantitative chemical shift MRI for bone marrow evaluation in the lumbar spine: a reproducibility study in healthy volunteers. J Comput Assist Tomogr 2001;25:691-7.
138. de Abreu MR, Wesselly M, Chung CB, Resnick D. Bone marrow MR imaging findings in disuse osteoporosis. Skeletal Radiol 2011;40:571-5.
139. Patsch JM, Li X, Baum T, Yap SP, Karampinos DC, Schwartz AV, Link TM. Bone marrow fat composition as a novel imaging biomarker in postmenopausal women with prevalent fragility fractures. J Bone Miner Res 2013;28:1721-8.
140. Baum T, Yap SP, Karampinos DC, Nardo L, Kuo D, Burghardt AJ, Masharani UB, Schwartz AV, Li X, Link TM. Does vertebral bone marrow fat content correlate with abdominal adipose tissue, lumbar spine bone mineral density, and blood biomarkers in women with type 2 diabetes mellitus? J Magn Reson Imaging 2012;35:117-24.
141. Lange MB, Nielsen ML, Andersen JD, Lilholt HJ, Vyberg M, Petersen LJ. Diagnostic accuracy of imaging methods for the diagnosis of skeletal malignancies: A retrospective analysis against a pathology-proven reference. Eur J Radiol 2016;85:61-7.
142. Shin DS, Shon OJ, Byun SJ, Choi JH, Chun KA, Cho IH. Differentiation between malignant and benign pathologic fractures with F-18-fluoro-2-deoxy-D-glucose positron emission tomography/computed tomography. Skeletal Radiol 2008;37:415-21.
143. Cheng C, Alt V, Pan L, Thormann U, Schnettler R, Strauss LG, Heinemann S, Schumacher M, Gelinsky M, Nies B, Dimitrakopoulou-Strauss A. Application of F-18-sodium fluoride (NaF) dynamic PET-CT (dPET-CT) for defect healing: a comparison of biomaterials in an experimental osteoporotic rat model. Med Sci Monit 2014;20:1942-9.
144. Cheng C, Alt V, Pan L, Thormann U, Schnettler R, Strauss LG, Schumacher M, Gelinsky M, Dimitrakopoulou-Strauss A. Preliminary evaluation of different biomaterials for defect healing in an experimental osteoporotic rat model with dynamic PET-CT (dPET-CT) using F-18-sodium fluoride (NaF). Injury 2014;45:501-5.
145. Cheng C, Heiss C, Dimitrakopoulou-Strauss A, Govindarajan P, Schlewitz G, Pan L, Schnettler R, Weber K, Strauss LG. Evaluation of bone remodeling with (18) F-fluoride and correlation with the glucose metabolism measured by (18)F-FDG in lumbar spine with time in an experimental nude rat model with osteoporosis using dynamic PET-CT. Am J Nucl Med Mol Imaging 2013;3:118-28.
146. Cheng C, Alt V, Dimitrakopoulou-Strauss A, Pan L, Thormann U, Schnettler R, Weber K, Strauss LG. Evaluation of new bone formation in normal and osteoporotic rats with a 3-mm femur defect: functional

assessment with dynamic PET-CT (dPET-CT) using 2-deoxy-2-[(18)F]fluoro-D-glucose ((18)F-FDG) and (18) F-fluoride. Mol Imaging Biol 2013;15:336-44.
147. Li J, Miller MA, Hutchins GD, Burr DB. Imaging bone microdamage in vivo with positron emission tomography. Bone 2005;37:819-24.
148. Frost ML, Blake GM, Cook GJ, Marsden PK, Fogelman I. Differences in regional bone perfusion and turnover between lumbar spine and distal humerus: (18)F-fluoride PET study of treatment-naïve and treated postmenopausal women. Bone 2009;45:942-8.
149. Uchida K, Nakajima H, Miyazaki T, Yayama T, Kawahara H, Kobayashi S, Tsuchida T, Okazawa H, Fujibayashi Y, Baba H. Effects of alendronate on bone metabolism in glucocorticoid-induced osteoporosis measured by 18F-fluoride PET: a prospective study. J Nucl Med 2009;50:1808-14.
150. Frost ML, Cook GJ, Blake GM, Marsden PK, Fogelman I. The relationship between regional bone turnover measured using 18F-fluoride positron emission tomography and changes in BMD is equivalent to that seen for biochemical markers of bone turnover. J Clin Densitom 2007;10:46-54.
151. Frost ML, Fogelman I, Blake GM, Marsden PK, Cook G Jr. Dissociation between global markers of bone formation and direct measurement of spinal bone formation in osteoporosis. J Bone Miner Res 2004;19:1797-804.
152. Cook GJ, Lodge MA, Blake GM, et al. Differences in skeletal kinetics between vertebral and humeral bone measured by 18F-fluoride positron emission tomography in postmenopausal women. J Bone Miner Res 2000;15:763-9.
153. Frost ML, Cook GJ, Blake GM, Marsden PK, Benatar NA, Fogelman I. A prospective study of risedronate on regional bone metabolism and blood flow at the lumbar spine measured by 18F-fluoride positron emission tomography. J Bone Miner Res 2003;18:2215-22.
154. Frost ML, Siddique M, Blake GM, Moore AE, Schleyer PJ, Dunn JT, Somer EJ, Marsden PK, Eastell R, Fogelman I. Differential effects of teriparatide on regional bone formation using (18)F-fluoride positron emission tomography. J Bone Miner Res 2011;26:1002-11.
155. Frost ML, Blake GM, Park-Holohan SJ, Cook GJ, Curran KM, Marsden PK, Fogelman I. Long-term precision of 18F-fluoride PET skeletal kinetic studies in the assessment of bone metabolism. J Nucl Med 2008;49:700-7.
156. Chesnut CH, Chesnut CH. Can PET-CT imaging and radiokinetic analyses provide useful clinical information on atypical femoral shaft fracture in osteoporotic patients? Curr Osteoporos Rep 2012;10:42-7.
157. Huovinen V, Saunavaara V, Kiviranta R, Tarkia M, Honka H, Stark C, Laine J, Linderborg K, Tuomikoski P, Badeau RM, Knuuti J, Nuutila P, Parkkola R.Vertebral bone marrow glucose uptake is inversely associated with bone marrow fat in diabetic and healthy pigs: [(18)F]FDG-PET and MRI study. Bone 2014;61:33-8.
158. Kogan F, Fan AP, McWalter EJ, Oei EH, Quon A, Gold GE. PET/MRI of metabolic activity in osteoarthritis: A feasibility study. J Magn Reson Imaging 2016. [Epub ahead of print].
159. Fechtenbaum J, Cropet C, Kolta S, Verdoncq B, Orcel P, Roux C. Reporting of vertebral fractures on spine X-rays. Osteoporos Int 2005;16:1823-6.
160. Cauley JA, Hochberg MC, Lui LY, Palermo L, Ensrud KE, Hillier TA, Nevitt MC, Cummings SR. Long-term risk of incident vertebral fractures. JAMA 2007;298:2761-7.
161. Liu M, Guo L, Pei Y, Li N, Jin M, Ma L, Liu Y, Sun B, Li C. Efficacy of zoledronic acid in treatment of osteoporosis in men and women-a meta-analysis. Int J Clin Exp Med 2015;8:3855-61.
162. Baur-Melnyk A. Malignant versus benign vertebral collapse: are new imaging techniques useful? Cancer Imaging Off Publ Int Cancer Imaging Soc 2009;9 Spec No A:S49-51.
163. Guglielmi G, Diacinti D, van Kuijk C, Aparisi F, Krestan C, Adams JE, Link TM. Vertebral morphometry: current methods and recent advances. Eur Radiol 2008;18:1484-96.
164. Oei L, Rivadeneira F, Ly F, Breda SJ, Zillikens MC, Hofman A, Uitterlinden AG, Krestin GP, Oei EH. Review of radiological scoring methods of osteoporotic vertebral fractures for clinical and research settings. Eur Radiol 2013;23:476-86.
165. Oei L, Ly F, El Saddy S, et al. Multi-functionality of computer-aided quantitative vertebral fracture morphometry analyses. Quant Imaging Med Surg 2013;3:249-55.
166. Genant HK, Wu CY, van Kuijk C, Nevitt MC. Vertebral fracture assessment using a semiquantitative technique. J Bone Miner Res 1993;8:1137-48.
167. Jiang G, Eastell R, Barrington NA, Ferrar L. Comparison of methods for the visual identification of prevalent vertebral fracture in osteoporosis. Osteoporos Int 2004;15:887-96.
168. Link TM, Guglielmi G, van Kuijk C, Adams JE. Radiologic assessment of osteoporotic vertebral fractures:

diagnostic and prognostic implications. Eur Radiol 2005;15:1521-32.
169. Ali RM, Green DW, Patel TC. Scheuermann's kyphosis. Curr Opin Pediatr 1999;11:70-5.
170. Hart ES, Merlin G, Harisiades J, Grottkau BE. Scheuermann's thoracic kyphosis in the adolescent patient. Orthop Nurs 2010;29:365-71; quiz 372-3.
171. Oei L, Estrada K, Duncan EL, et al. Genome-wide association study for radiographic vertebral fractures: a potential role for the 16q24 BMD locus. Bone 2014;59:20-7.
172. Oei L, Zillikens MC, Rivadeneira F, Oei EH. Osteoporotic Vertebral Fractures as Part of Systemic Disease. J Clin Densitom 2016;19:70-80.
173. Oei L, Zillikens MC, Rivadeneira F, Oei EH. Genetics of Osteoporotic Vertebral Fractures. J Clin Densitom 2016;19:23-8.
174. Makurthou AA, Oei L, El Saddy S, Breda SJ, Castaño-Betancourt MC, Hofman A, van Meurs JB, Uitterlinden AG, Rivadeneira F, Oei EH. Scheuermann disease: evaluation of radiological criteria and population prevalence. Spine (Phila Pa 1976) 2013;38:1690-4.
175. Breda SJ, Oei HD, Oei EH, Zillikens MC. Osteoporotic vertebral fractures or Scheuermann's disease?. Ned Tijdschr Geneeskd 2013;157:A6479.
176. Armbrecht G, Felsenberg D, Ganswindt M, Lunt M, Kaptoge SK, Abendroth K, Aroso A, Banzer D, Bhalla AK, Dequeker J, Eastell R, Hoszowski K, Lyritis G, Delmas PD, Masaryk P, Miazgowski T, Cannata J, Nuti R, Oei L, Poor G, Redlund-Johnell I, Reid DM, Reisinger W, Schatz H, Todd CJ, Woolf AD, Javaid K, Rivadeneira F, Silman AJ, Cooper C, O'Neill TW, Reeve J; European Vertebral Osteoporosis Study and European Prospective Osteoporosis Study Groups. Vertebral Scheuermann's disease in Europe: prevalence, geographic variation and radiological correlates in men and women aged 50 and over. Osteoporos Int 2015;26:2509-19.

Cite this article as: Oei L, Koromani F, Rivadeneira F, Zillikens MC, Oei EH. Quantitative imaging methods in osteoporosis. Quant Imaging Med Surg 2016;6(6):680-698. doi: 10.21037/qims.2016.12.13

